Controlling the porosity of fibrous scaffolds by modulating the fiber diameter and packing density

Sherif Soliman,[1,2,3] Shilpa Sant,[2,3] Jason W. Nichol,[2,3] Masoud Khabiry,[2,3] Enrico Traversa,[1] Ali Khademhosseini[2,3]

[1]Department of Chemical Sciences and Technology, University of Rome Tor Vergata, Via della Ricerca Scientifica 1, 00133 Rome, Italy
[2]Harvard-MIT Division of Health Sciences and Technology, Massachusetts Institute of Technology, Cambridge, Massachusetts 02139
[3]Center for Biomedical Engineering, Department of Medicine, Brigham and Women's Hospital, Harvard Medical School, Boston, Massachusetts 02115

Received 6 December 2009; revised 18 October 2010; accepted 27 October 2010
Published online 10 January 2011 in Wiley Online Library (wileyonlinelibrary.com). DOI: 10.1002/jbm.a.33010

Abstract: Porosity has been shown to be a key determinant of the success of tissue engineered scaffolds. A high degree of porosity and an appropriate pore size are necessary to provide adequate space for cell spreading and migration as well as to allow for proper exchange of nutrients and waste between the scaffold and the surrounding environment. Electrospun scaffolds offer an attractive approach for mimicking the natural extracellular matrix (ECM) for tissue engineering applications. The efficacy of electrospinning is likely to depend on the interaction between cells and the geometric features and physicochemical composition of the scaffold. A major problem in electrospinning is the tendency of fibers to accumulate densely, resulting in poor porosity and small pore size. The porosity and pore sizes in the electrospun scaffolds are mainly dependent on the fiber diameter and their packing density. Here we report a method of modulating porosity in three dimensional (3D) scaffolds by simultaneously tuning the fiber diameter and the fiber packing density. Nonwoven poly(ε-caprolactone) mats were formed by electrospinning under various conditions to generate sparse or highly dense micro- and nanofibrous scaffolds and characterized for their physicochemical and biological properties. We found that microfibers with low packing density resulted in improved cell viability, proliferation and infiltration compared to tightly packed scaffolds. © 2011 Wiley Periodicals, Inc. J Biomed Mater Res Part A: 96A: 566–574, 2011.

Key Words: electrospinning, poly(ε-caprolactone), tissue engineering, scaffold, porosity, pore size

INTRODUCTION

Tissue engineering is an interdisciplinary field that strives to generate replacement tissues to improve the function of diseased or damaged organs.[1,2] In one approach, tissue engineering involves the expansion of cells *ex vivo* followed by seeding onto a biodegradable scaffold, which mimics the natural tissue architecture, prior to implantation. Ideally, these scaffolds should promote cellular adhesion, proliferation, and migration while having similar structure and mechanical properties to the tissue that they aim to replace.[3–5] Various methods have been described for preparing porous tissue engineering scaffolds such as by particle leaching,[6,7] emulsion freeze-drying,[8] and phase separation.[7,9] However, despite significant advances, potential limitations include lack of desired mechanical stability and porosity.

In the past few years, electrospinning has emerged as a promising technique for manufacturing fibrous scaffolds with a large surface area to volume ratio to mimic the topology of the native ECM.[10–15] Electrospinning of polymeric biomaterials has generated much interest since it can be used to fabricate tissue engineering scaffolds with nanoscale resolution in a rapid and cost-effective manner. In the electrospinning process, a solution containing a polymer dissolved in an appropriate solvent is ejected through a nozzle by electrostatic attraction to generate ultrafine fibers, which are deposited onto a grounded metal collector.[16] The resultant structure is a randomly oriented micro- or nanofiber network mesh with a highly open porous architecture. The morphology of fibers can be controlled with various parameters in the electrospinning process, such as solution properties (i.e., viscosity, conductivity, polymer molecular weight), process parameters (i.e., flow rate, applied potential), and ambient conditions (i.e., temperature, humidity).[17]

The efficacy of this approach is likely to depend on the interaction between cells and the physico-chemical composition of the scaffold. In this respect, a highly porous structure is required to allow for cellular infiltration and ensure the exchange of nutrients and oxygen as well as waste products between the seeded cells and the surrounding environment. A major concern in electrospun scaffolds is the tendency to accumulate densely packed fibers, resulting in poor porosity hindering cellular infiltration inside the scaffolds, thus, limiting their potential for 3D tissue engineering applications. While many studies have been reported on

Correspondence to: A. Khademhosseini; e-mail: alik@rics.bwh.harvard.edu

 © 2011 WILEY PERIODICALS, INC.

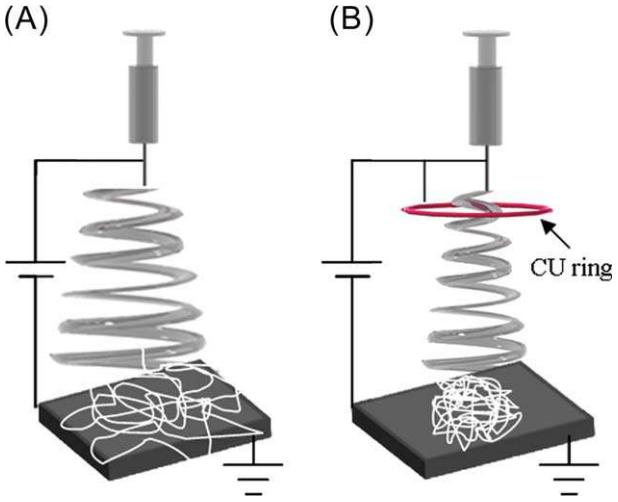

FIGURE 1. Schematic representation of the electrospinning setup (A) without a ring (basic setup), (B) with a positively charged Cu ring. [Color figure can be viewed in the online issue, which is available at wileyonlinelibrary.com.]

modulating the geometrical structures of the scaffolds, only a few studies have investigated the effects of pore size and shape on cell adhesion and proliferation.[18–22] Culture of cells on scaffolds with poor porosity often results in formation of a monolayer of cells, rather than a well seeded 3D scaffold. Poor cellular infiltration has been attributed to pore diameters that are orders of magnitude smaller than the dimensions of the cell.[23–25] Oxygen and nutrient diffusion limitations also hinder the penetration distance of cells.[26] As a result, cells are only able to survive close to the surface. Interconnectivity between pores is another critical factor in promoting the migration and infiltration of cells into the scaffold.

The porosity and pore sizes in electrospun scaffolds are dependent upon the fiber diameter and their packing density. In electrospinning, control of the fiber diameter is easy to achieve by tuning the properties of the polymer solution and the processing conditions.[23,27] In contrast controlling the packing density of the electrospun fibers is a much more difficult task. The objective of this study was to simultaneously modify the diameter and packing density of fibers to tune the average pore size and overall porosity of the electrospun scaffolds. By improving both the overall porosity and average pore size it was hypothesized that cell spreading, proliferation, and infiltration into the scaffolds would be improved. Poly(ε-caprolactone) (PCL) was used as the base material for this study due to its biocompatibility and strong mechanical integrity. In addition, PCL is a suitable candidate material for short-term load-bearing applications due to its slow degradation rate *in vivo*.[28]

MATERIALS AND METHODS

Materials

All chemicals were purchased from Sigma-Aldrich (Sigma, St. Louis, MO), and all biological supplies were purchased from Invitrogen (Gaithersburg, MD) unless otherwise noted.

Electrospinning apparatus

The electrospinning setup consisted of a programmable syringe pump (Model R99-E, Razel Scientific Instruments) attached to a plastic syringe with a flat ended needle connected to a positive terminal of a high voltage power supply (0–30 kV) (EN 61010-1, Glassman High Voltage). The fibers were collected on a square stainless-steel grounded plate (dimensions: 11 cm × 11 cm × 0.5 cm). In addition to the basic setup, an auxiliary copper ring (15 cm diameter) was placed 4 cm below the capillary tip and connected to the positive terminal of the power supply in order to achieve higher packing density (Fig. 1).

PCL solutions

PCL polymer solutions were prepared using a 7:1 volume ratio of chloroform:methanol. Table I provides a summary of the polymer compositions and processing parameters used in this study. The resulting scaffolds at the given conditions were classified as (a) microfibers with low fiber density (M-LD), (b) microfibers with high fiber density (M-HD) (c) nanofibers with low fiber density (N-LD) and (d) nanofibers with high fiber density (N-HD). The auxiliary ring was employed to achieve a high packing density (HD) and was deactivated to produce scaffolds with low packing density (LD). Scaffolds were spun to a thickness of 50–60μm and dried overnight in a desiccator to remove any remaining solvent prior to further use. All samples for material and biological characterization consisted of 10 mm discs die-punched from larger sheets.

Material characterization

Scanning electron microscopy (SEM). Electrospun scaffolds were dried and sputter-coated with gold for 2 min and their microscopic structures were observed with a scanning electron microscope (SEM) (JEOL 6320FV) at an acceleration voltage of 10 kV. SEM micrographs were used to measure the fiber diameter of the electrospun scaffolds. High magnification images (5000×) were taken of random

TABLE I. Electrospinning Process Conditions to Generate Various Types of Scaffolds

Scaffold Classification	Concentration (wt %)	Collector Distance (cm)	Voltage (kV)	Flow Rate (mL h^{-1})	Needle Gauge	Auxiliary Ring	Spinning Time (min)
M-HD	15	16.5	12	4	18	+	15
M-LD	15	24	20	4	18	−	20
N-HD	10	16.5	12	8	21	+	15
N-LD	10	24	20	8	21	−	20

fields of the scaffolds. Means and root mean square errors (RMS) of each sample of the fiber populations reported in Figure 3(A). A set of 50 or more random measurements were taken of the fibers appearing in the top layer of SEM micrographs by manually identifying the edges of the fibers in the image and quantifying the number of pixels per fiber using Spot Imaging Software Advanced (Diagnostic Instruments, Sterling Heights, USA).

Porosity measurements. The porosity (ε) of the scaffolds was measured at room temperature by using the liquid intrusion method.[17] Briefly, the electrospun scaffolds were weighed and subsequently immersed in ethanol overnight on a mechanical shaker to allow the liquid to penetrate into the scaffold voids. The density of ethanol (ρ_{ETH}) is 0.789 g mL^{-1} while the density of PCL (ρ_{PCL}) is 1.45 g cm^3. The surface of the samples was then dried blotted dry and weighed once more to determine the mass of ethanol present within the scaffold. Measurements were made on five samples of each scaffold type. The porosity was calculated as

$$\varepsilon = V_{ETH}/(V_{ETH} + V_{PCL}) \tag{1}$$

V_{ETH} is the volume of intruded ethanol and was calculated as the ratio between the observed mass change after intrusion and ρ_{ETH}. V_{PCL} is the volume of the PCL fibers and was calculated as the ratio between the dry scaffold mass before intrusion and ρ_{PCL}.

Pore size estimate. The pore size estimate was pursued indirectly through approximate statistical models similar to other studies.[9] The elegant model by Eichhorn and Sampson[11] allows one to obtain the 3D pore radii "$\bar{r}$" associated to a unimodal fiber distribution. The average pore radius "$\bar{r}$" can be calculated from Eq. (2)

$$\bar{r} = \int_0^\infty \psi(r)dr \tag{2}$$

where $\psi(r)$ can be obtained from the following equation:

$$\psi(r) = \frac{4\beta}{\varepsilon \ln\left(\frac{1}{\varepsilon}\right)\pi\omega\rho_{PCL}} \sqrt[k]{\left[\frac{\Gamma(k, bn)}{\Gamma(k)}\right]^{n-k}} \frac{r^k}{e^{br}} \tag{3}$$

In Eq. (3), Γ (k, bn) and Γ (k) are the incomplete and complete gamma functions respectively, k is a constant parameter equal to 1.6, n is an equivalent number of layers $n = \frac{4\beta}{\pi\omega\rho_{PCL}\ln(1/s)}$, and b is an experimental parameter. The latter is defined as $b = 2k/(r)$ as a function of the average bidimensional pore diameter $\langle r\rangle$ of one fiber layer, which in turn is related to ε and to the average ω by

$$\langle r\rangle \cong \left(\frac{\pi\sqrt{\pi}}{8\ln(1/\varepsilon)} - \frac{\sqrt{\pi}}{4}\right)\omega \tag{4}$$

With the first model or by second model as:

$$\langle r\rangle \cong \frac{\omega}{\ln(1/\varepsilon)} \tag{5}$$

providing for an alternative estimate of $\langle r\rangle$ in place of Eq. (4). Both models were implemented and reflected in Figure 3.

Mechanical testing. Tensile tests were performed on 5 × 20 mm^2 rectangular strips cut from 50-μm scaffold sheets. The mechanical properties of the samples were compared using an Instron 5542 mechanical testing system (Instron, Norwood, MA). Samples were loaded at a rate of 10%/min until failure. The testing routine was performed three times for each sample and the results were averaged.

Biological methods

Culture of human umbilical vein endothelial cells (HUVECs). GFP-HUVEC cells (HUVEC cells transfected to express green fluorescent protein, GFP) were a kind gift from the laboratory of Dr. Judah Folkman, Children's Hospital, Boston. The cells were cultured in EBM-2 (Endothelial Cell Basal Medium-2, Lonza, MD) supplemented with the provided growth factor kit. The cell cultures were maintained at 37°C and 5% CO_2 and media was changed twice each week.

Cell imaging. Disc-shaped PCL scaffolds (diameter 10 mm, height 50 μm) were prepared using a biopsy punch and subsequently degassed under vacuum for 24 h. The scaffolds were sterilized in a 70% ethanol solution overnight and pre-incubated in EBM-2 for 12 h prior to cell seeding. The discs were secured in 24-well culture plates using Vitron O-rings (Aldrich, USA). Cells were trypsinized, washed with phosphate-buffered saline (PBS) and seeded at a density of 1 × 10^5 cells/well/mL. Following a 12 h attachment period in complete EBM-2 medium, the supernatant was removed and replaced with fresh medium. The cells were fixed at day 4 post-seeding in a 4% formaldehyde solution for 1 h, followed by three washes with PBS. The samples were then dehydrated using increasing concentrations of ethanol (25, 50, 75, 85, 95, and 100%). Observation of cell surface distribution was performed using SEM and inverted fluorescence microscopy. Samples for SEM were subsequently treated as described for cell-free SEM specimens. Fluorescence microscopy was performed to evaluate the surface distribution of seeded cells using an inverted fluorescence microscope (Nikon Eclipse Ti, Avon, USA). The distribution of the cells within the scaffolds was evaluated by confocal laser scanning microscopy (LSM). Endogenous GFP expression was counterstained with 4′,6′-diamidino-2-phenylindole (DAPI, present in Vectashield® mounting medium; Vector Labs, Canada). Whole mount samples were imaged using an Olympus FV-1000 LSM.

Evaluation of cell proliferation on PCL fibrous scaffolds. Cell proliferation was measured using continuous AlamarBlue® assay (AB, Invitrogen, USA) on days 2, 4, and 6 post-seeding

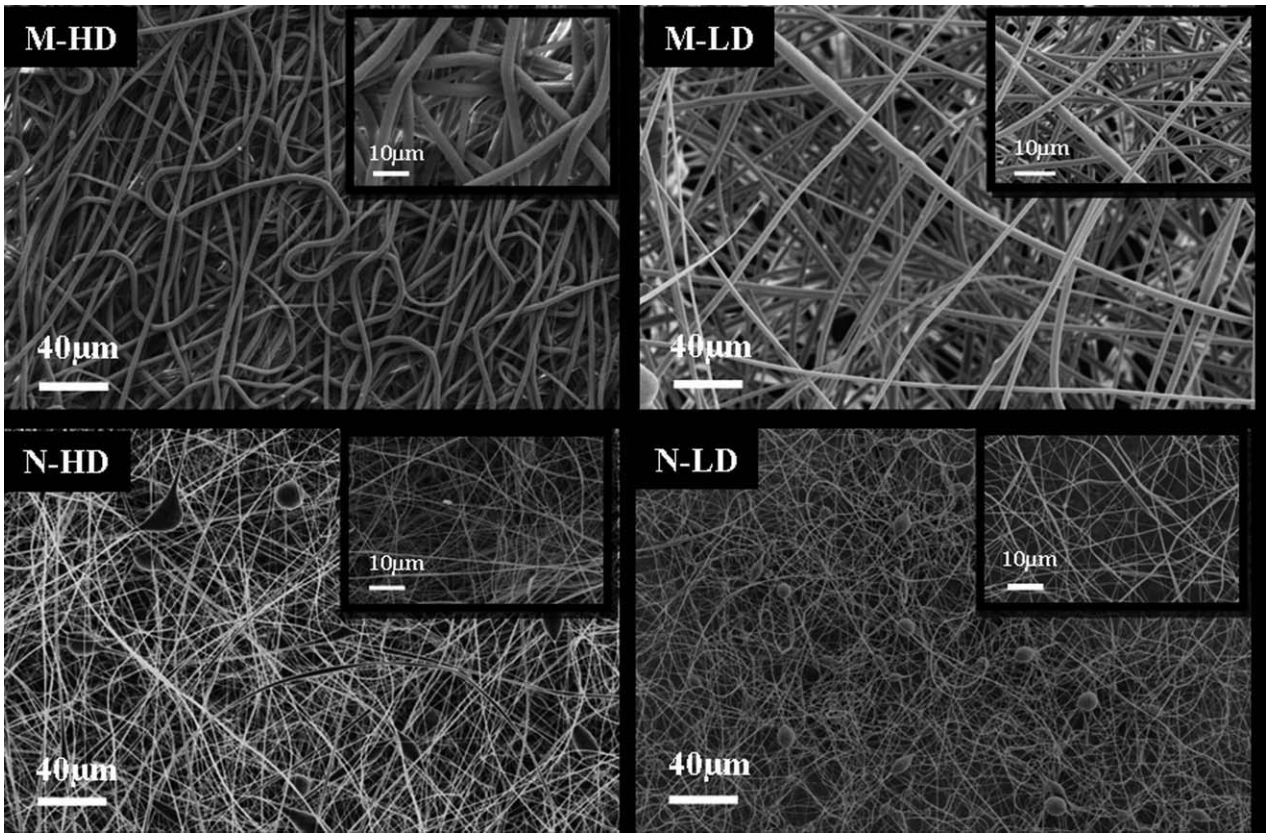

FIGURE 2. Scanning electron micrographs of electrospun fibers consisting of the four scaffold types tested. Original magnification is ×1000. Inset in each figure shows higher magnification (×5000 for M-HD, N-HD, N-LD and ×2000 for M-LD).

as previously described.[29] After initial seeding in EBM-2 media, at each time point, supernatants were removed and 1 mL fresh medium containing 5% (v/v) AB was added into each well. After various incubation periods, triplicate 100-μL aliquots of AB containing medium were moved into a 96-well plate for absorbance measurement at 570 nm. An equal volume of fresh medium without AB was added to each well.

RESULTS AND DISCUSSION

In this study we determined the conditions necessary to generate nano- or microfibers with low or high packing density and subsequently analyzed the effect of each of these factors on cell migration, proliferation, and infiltration. A range of parameters were optimized to obtain smooth and uniform fibers in all scaffold groups. The parameters shown in Table I were selected as the optimal conditions for obtaining reproducible randomly oriented uniform meshes of nano- and microfibers.

Morphological analysis

A common solvent used for electrospinning of PCL is chloroform. However, we observed that chloroform produced an unstable Taylor cone, leading to irregular fiber formation. It has been previously reported that adding methanol to the chloroform increases the conductivity of the solution and leads to a more stable Taylor cone.[17] Changing the solvent from chloroform to a 7:1 mixture of chloroform: methanol produced a stable spinning jet and thus, resulted in the formation of smooth fibers. In these experiments the fiber diameter was found to be strongly influenced by the concentration of the polymer in solution. Specifically, increasing the concentration of the polymer solution resulted in increased fiber diameters. At the processing conditions explored in this work, micro- and nanofibers were formed at 15% (w/v) and 10% (w/v), respectively. The internal diameter of the needle was also found to have a slight effect on the resultant fiber diameter, with a smaller internal diameter producing smaller diameter fibers. The internal diameter was also observed to have an effect on bead formation. Specifically, we found that 18- and 23-G needles could be used to generate micro- and nano-fibers, respectively without bead formation. As shown in the SEM images of Figure 2, a relatively uniform fiber diameter was formed suggesting a high degree of reproducibility. The mean diameter and RMS of the fiber diameter distributions of each group are reported in Figure 3A.

The packing density of the fibrous meshes could be modulated either by varying the distance between the tip of the needle and collecting plate or by operating with the auxiliary ring. The working distance between the tip of the needle and collector has a direct impact on the flight time and on the strength of the electric field driving the motion of the fiber. The winding path of the spinning jet was

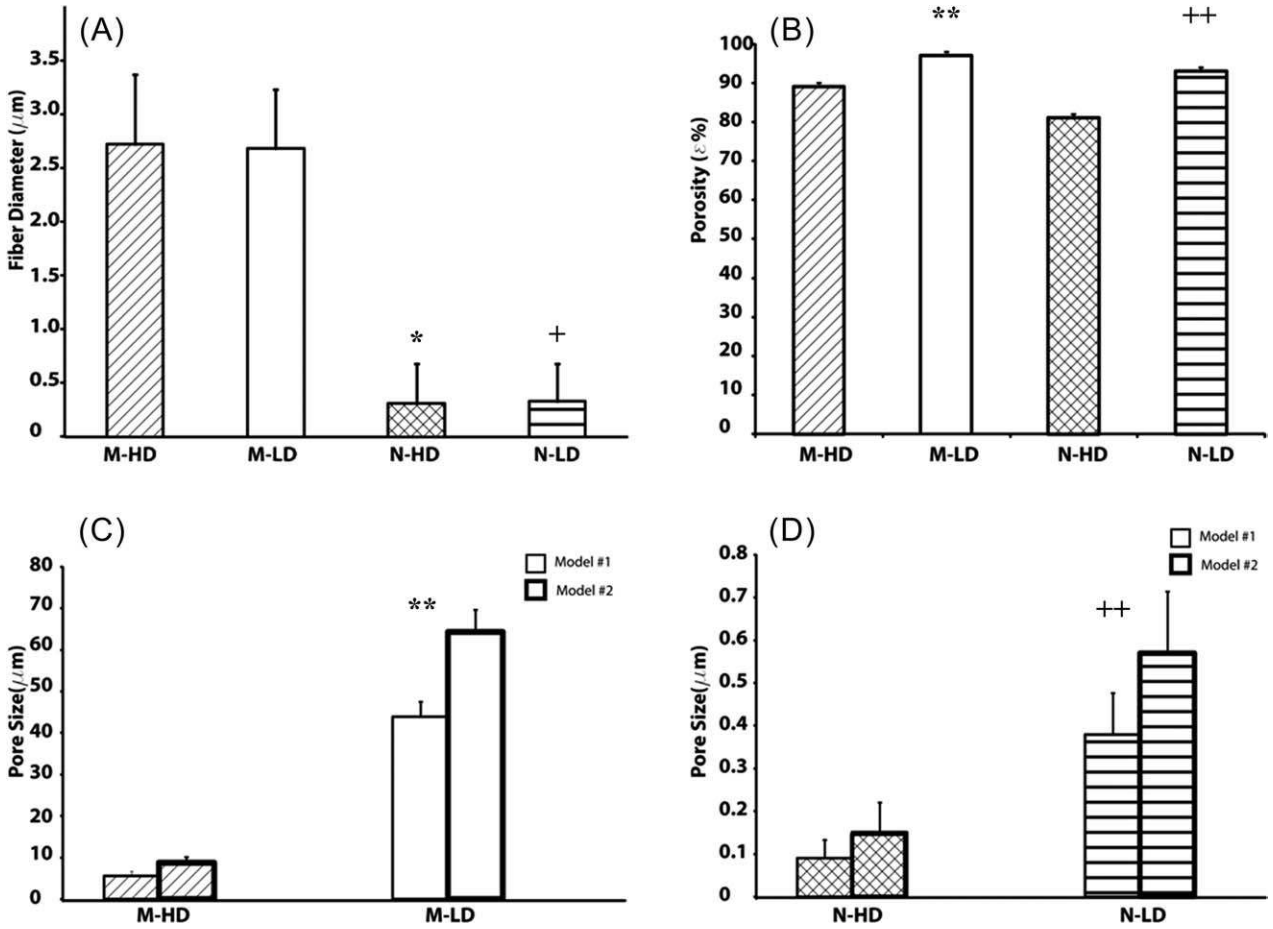

FIGURE 3. Mean and root mean square errors for the: (A) fiber diameter [ω] measurements, (B) porosity [ε], (C, D) pore size [2] estimates for micro- (C) and nanofibers (D). Statistically significant differences at $p < 0.05$, *M-HD vs. N-HD, **M-HD vs. M-LD, $^{+}$M-LD vs. N-LD, $^{++}$N-HD vs. N-LD (Student's *t* test).

observed to widen as it traveled further from the needle. Thus, by reducing the working distance, the jet was observed to contact the collecting plate before it could widen, resulting in a more concentrated fibrous sheet in a smaller area.

A conductive auxiliary ring was also used to increase the fiber packing density. The presence of a positively charged ring forces the similarly charged fibers to follow a more focused path near the center of the ring due to repulsive forces. This resulted in the fibrous mat formation in a confined circular space, rather than over the entire collector area. It was necessary to increase the collector distance when using the auxiliary ring to compensate for the increased voltage required for this mode of operation to maintain a stable jet. To generate the desired scaffold thickness, the spinning time was varied on a case-by-case basis; namely it was reduced when high density scaffolds were made via the use of the auxiliary ring. For our purposes, all scaffolds were made with a comparable thickness that ranged from 50 to 60 μm (as measured with a digital micrometer with a precision of 1 μm).

To determine the porosity of each of the scaffold types, the average estimates of porosity $\varepsilon_{\%}$ was determined by using liquid intrusion analysis [Fig. 3(B)]. The porosity appeared to decrease with increasing the weight of the scaffolds and the fiber diameters. This was also confirmed by the SEM images. We also performed pore size modeling using two commonly used methods since experimental approaches such as mercury porosimetry could not be applied to our scaffolds due to high pressure.[17] The representative pore sizes computed from these models (by arbitrarily using the liquid inclusion measures of ε as input) are shown in Figure 3(C,D) for each scaffold material. Both models showed consistent results for the different scaffold types. However, model no. 1 estimated slightly smaller values than those from model no. 2. The pore size in the tested scaffolds was found to be mainly dependant on the fiber diameter and their packing density. The larger pore size is obtained with larger fiber diameter. Also, the lower fiber packing density resulted in the higher pore size. As a result, the M-LD was found to have a significantly larger pore size (~44–64 μm) than the other considered scaffolds.

Mechanical properties

To further characterize the effect of fiber diameter and porosity on bulk mechanical properties of electrospun

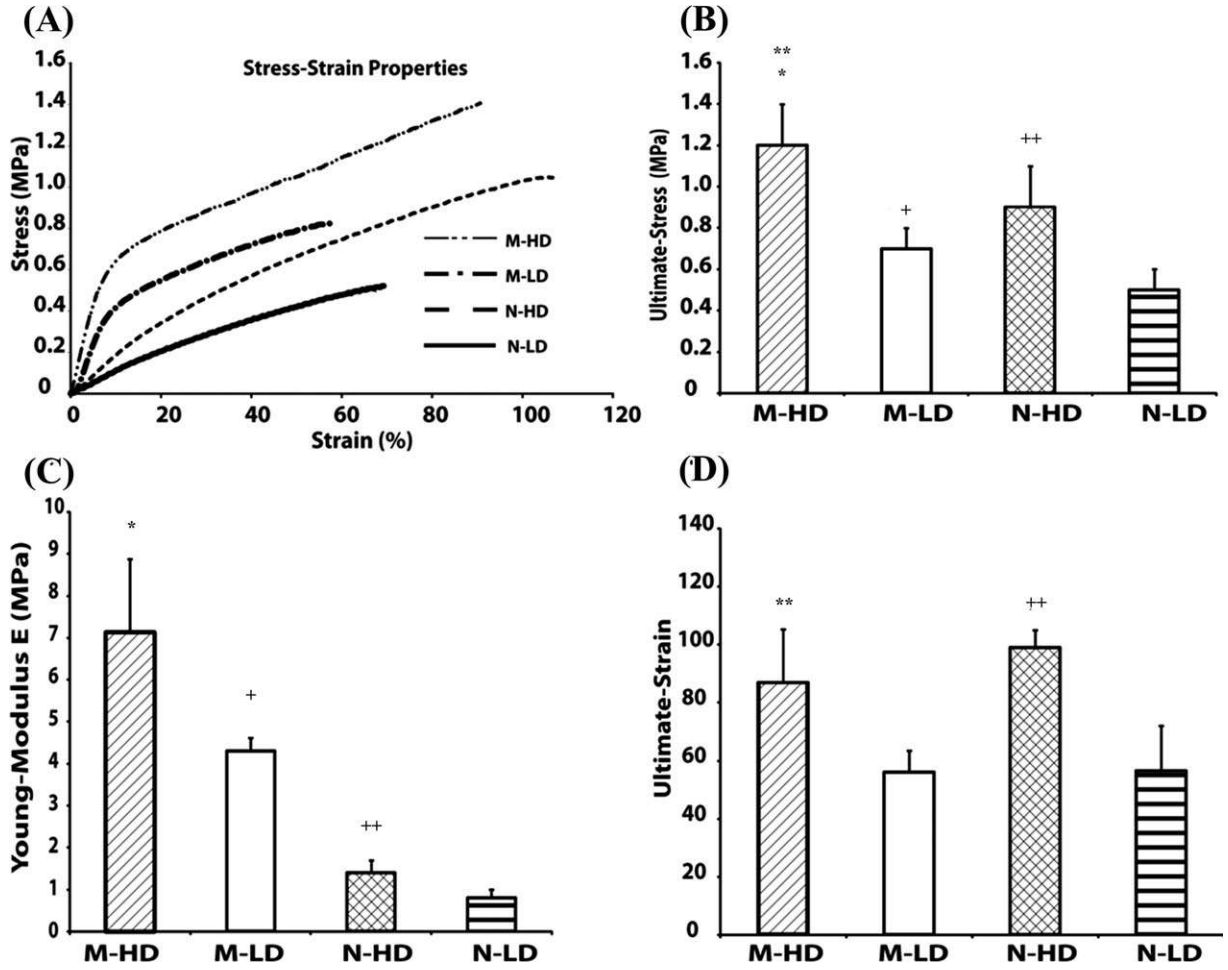

FIGURE 4. Mechanical characterization of the micro- and nanofibrous electrospun PCL scaffolds. (A) Representative stress–strain curves, (B) Ultimate stress measurements, (C) Young's Modulus, (D) Ultimate strain measurements. Statistically significant differences at $p < 0.05$, *M-HD vs. N-HD, **M-HD vs. M-LD, $^{+}$M-LD vs. N-LD, $^{++}$N-HD vs. N-LD (Student's *t* test).

scaffolds, we performed a range of mechanical analysis. Interestingly, while the general stress–strain behaviors of the different scaffold types were comparable (Fig. 4), the scaffolds made of densely packed fibers were more mechanically robust compared to their low density counterparts. Specifically, the ultimate stress was significantly higher in densely packed scaffolds as compared to the low density scaffolds, while, in general, the micrometer scale fibers outperformed the matched nanometer scale fibers [Fig. 4(B)]. The stiffness, as measured by the Young's Modulus, decreased in the following order M-HD, M-LD, N-HD, and N-LD, with all conditions being significantly different than each other [Fig. 4(C)]. The material ductility also increased in a similar fashion as the ultimate stress, with densely packed fibers being significantly more extensible [Fig. 4(D)]. The softening behavior reflecting different failure modes demonstrate that, while structures composed of dense fibers behave as multilayer composites failing by delamination from mode II crack, scaffolds composed of less densely packed fibers behave as fiber bundles failing by mode I crack.

The decreases in ultimate stress and strain, as well as Young's Modulus, from high to low density packing were all roughly in the range of 30–50%, which was similar to the range of increase in the average pore size for the same conditions. This suggests that ultimate stress, ultimate strain and Young's Modulus are all roughly proportional to the pore size for electrospun scaffolds created using the described techniques. Further experimental and statistical analysis would be necessary to determine the characteristics of these relationships as well as to determine the range of pore sizes for which these relationships remain valid. While overall porosity also increased a small amount in the sparsely packed cases, this change was not as pronounced as the change in pore size, making this effect less likely to correlate with the observed changes in mechanical properties. However, further evaluation would be necessary to determine the relative role that overall porosity played in the observed changes in mechanical properties.

Biological validation

Cell morphology. To analyze the long term response of cells to various types of scaffolds, endothelial cells were seeded on scaffolds and their morphology was analyzed. Following 12 days of culture, the scaffolds containing seeded

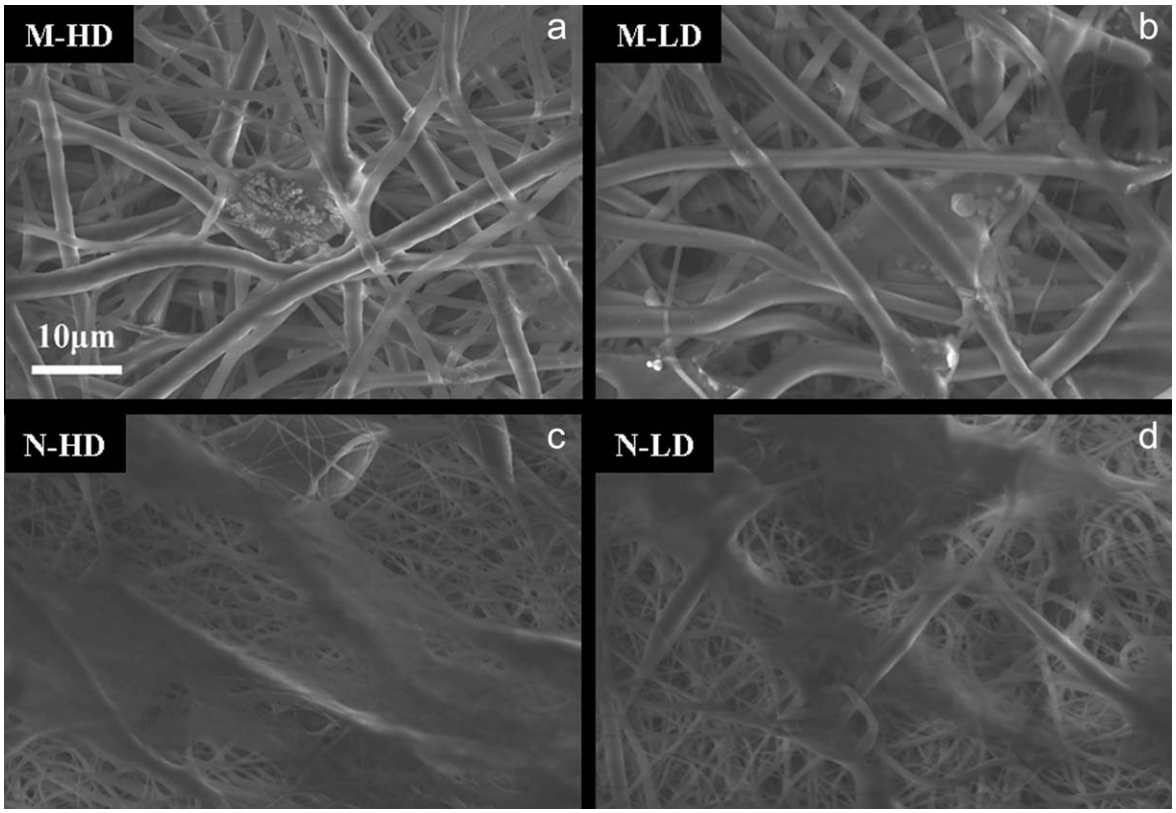

FIGURE 5. SEM images of electrospun fibers with HUVEC cells after 4 days of culture, for (a) M-HD, (b) M-LD, (c) N-HD, and (d) N-LD scaffolds.

endothelial cells were fixed, and the morphology of cells was investigated by means of SEM. As shown in Figure 5, endothelial cells adhered and aligned on all different types of scaffolds that were analyzed. A visible interaction between the cells and fibers was observed in the samples containing microfibers where the cells had the tendency to align on the individual fibers and bridge between adjacent fibers as shown previously.[30,31] This is likely due to the fact that the cellular, fiber diameter and average pore size were all in the micron range, making the cells able to bind across individual pores and align along individual fibers. As expected, since the pore size was on the order of microns, cells could be seen penetrating below the surface of the scaffold. Conversely, on the nanofibrous scaffolds cells seemed to grow randomly rather than aligning in any way, and exhibited minimal capability to infiltrate into the surface due to the average pore size being many times smaller than the dimensions of the cells. Similarly, cells could not bind only to individual fibers due to their small size, which being in the nanoscale were likely too small for the cells to easily differentiate.

Cell viability. To further characterize the cell behavior on the electrospun scaffolds, the metabolic activity of cells seeded on the electrospun fibers was evaluated using Alamar Blue (AB) assay. AB staining measures metabolic activity of cells on a scaffold, which often correlates to the number of cells and can thus be used to determine the rate of cellular proliferation. It is well established that cell adhesion and spreading play important roles in cell viability and proliferation, and as cell spreading and adhesion varied between the groups, viability and proliferation could vary as well.[32] Figure 6 shows the AB absorbance measurements on the various PCL scaffolds on days 2, 4, and 6. Scaffolds showed significant differences in cell proliferation as a function of fiber diameter, fiber packing density as well as

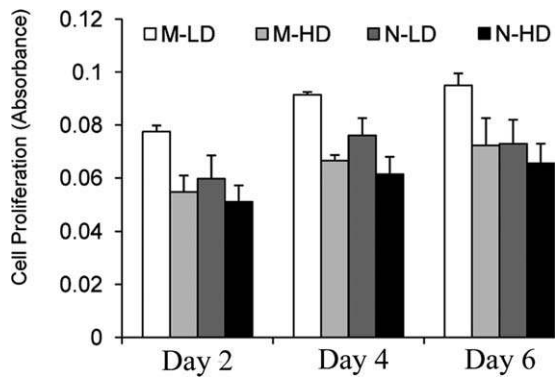

FIGURE 6. Cell proliferation of HUVEC cells by Alamar blue assay on different scaffolds as a function of culture time. Cell proliferation showed significant differences between different scaffolds and as a function of culture days ($p < 0.05$, two-way ANOVA followed by post-hoc Tukey test). M-LD showed significantly faster proliferation as compared to M-HD, N-LD, and N-HD. Similarly, N-LD showed higher proliferation than n-HD ($p < 0.05$, post-hoc Tukey test). For the same scaffolds, proliferation increased significantly from day 2 to day 4 and day 6 ($p < 0.05$, two-way ANOVA, post-hoc Tukey test).

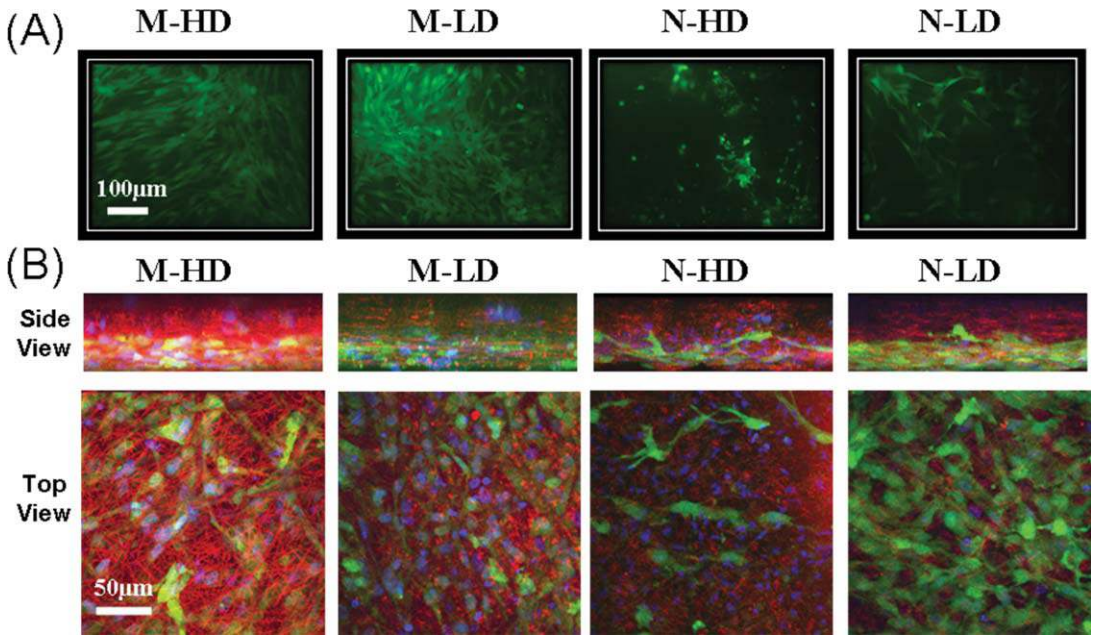

FIGURE 7. Analysis of cell infiltration into electrospun scaffolds. (A) Fluorescent microscopic images of GFP-HUVECs at day 7. Images were taken with the ×20 objective. (B) 3D images (at ×60) of the scaffolds by confocal microscopy. [Color figure can be viewed in the online issue, which is available at wileyonlinelibrary.com.]

number of days in culture ($p < 0.05$, two-way ANOVA, post-hoc Tukey test). To evaluate the effect of fiber diameter on cell proliferation, we compared microfibrous scaffolds with nanofibrous scaffolds. It was observed that cell proliferation on the microfibrous mats was higher than nanofibrous mats similar to previously published reports.[24,32,33] Some authors have also reported that focal adhesion complexes, which are larger than 1 μm, are involved in cell adhesion to biomaterials.[24,32,33] This implies that nanofibers may not provide sufficient surface area for cell adhesion and spreading, thus, affecting cell viability and proliferation.

It is interesting to note that only micro- and nanofibrous scaffolds with low fiber density (M-LD and N-LD, respectively) showed significant differences (student's paired t test, $p < 0.05$) whereas increasing fiber density of the scaffold counteracted this effect as evident from marginal differences between M-HD and N-HD ($p > 0.05$). It was apparent that fiber density played an important role in cell proliferation into nonwoven fibrous scaffolds. Again, microfibrous scaffolds with low fiber density (M-LD) showed a significantly higher rate of proliferation than those with high fiber density (M-HD) (student's paired t test, $p < 0.05$). Similarly, nanofibrous scaffolds with low fiber density (N-LD) showed higher proliferation than those with high fiber density (N-HD) when the scaffold density was changed. However, these differences were not significant, due to fiber density effects (N-LD vs. N-HD, student's paired t test, $p > 0.05$). This seems plausible as decreased fiber density of the scaffold resulted in less packed nonwoven mats. This would lead to greater inter-pore distance and more space for cells to migrate and proliferate inside the scaffolds. This effect was more pronounced in microfibrous scaffolds as larger diameter also led to increased inter-pore distance. These results clearly underline the synergistic effect of large fiber diameter and low fiber density in the electrospun nonwoven mats.

Cell distribution. To further characterize the infiltration of cells into electrospun scaffolds, we analyzed the distribution of cells on different type scaffolds. For microscopic observations, cell-laden scaffold samples were observed under inverted fluorescence microscope after days 1, 3, 5, and 7 (data not shown). Consistent with AB assay, microfibrous, and nanofibrous scaffolds with low fiber density (M-LD and N-LD) showed higher number of cells as compared to high density fibers [Fig. 7(A)].

The distribution of cells inside the scaffolds was also studied by confocal laser scanning microscopy. It was observed that all the scaffolds formed a monolayer of cells on their surface at the end of day 12. However, both micro- and nanofibrous scaffolds with low fiber density clearly showed densely packed cells up to half of the scaffold height [Fig. 7(B), M-LD and N-LD]; while scaffolds with high fiber density generated a single monolayer of cells at the top of the scaffolds [Fig. 7(B), M-HD and N-HD]. This is due to the effect of fiber packing density. At low fiber packing density, the porosity of scaffolds is high to allow cells to migrate and proliferate inside the scaffolds and form thick layers. However, when initial fiber packing density is high, cells can only migrate and proliferate horizontally and not vertically. Once this space is filled up, cells could not penetrate deeper inside the scaffolds. The M-LD scaffold exerted the maximum adhesion rate of cells and their proliferation when compared with the other considered scaffolds. This is evident from confocal images and the AB assay test results.

These results are in accordance with other authors where cell infiltration within the scaffolds increased with increasing fiber diameter and hence the pore sizes of the scaffolds.[23]

CONCLUSIONS

In this work, we performed a study to simultaneously analyze the effect of fiber diameter and fiber packing density on scaffold mechanical and biological properties. By modulating the electrospinning process conditions, four different groups of scaffolds were produced consisting of: (a) microfibers with low fiber density (M-LD), (b) microfibers with high fiber density (M-HD), (c) nanofibers with low fiber density (N-LD), and (d) nanofibers with high fiber density (N-HD). The mechanical tensile test results showed that scaffolds with higher packing density of fibers had higher strength and failed by delamination; while scaffolds with low packing fiber density failed under mode I crack. The biological validation of the scaffolds demonstrated that both micro- and nanofibrous scaffolds with low fiber density clearly showed a better cell proliferation and infiltration within the scaffolds as compared with the highly dense scaffolds. A scaffold consisting of microfibers with a low packing density exhibited maximum cell adhesion and proliferation rate compared with the other scaffolds under consideration.

REFERENCES

1. Khademhosseini A, Vacanti JP, Langer R. Progress in tissue engineering. Sci Am 2009;300:64–71.
2. Langer R, Vacanti JP. Tissue engineering. Science 1993;260: 920–926.
3. Khademhosseini A, Bettinger C, Karp JM, Yeh J, Ling Y, Borenstein J, Fukuda J, Langer R. Interplay of biomaterials and micro-scale technologies for advancing biomedical applications. J Biomater Sci Polym Ed 2006;17:1221–1240.
4. Khademhosseini A, Langer R, Borenstein J, Vacanti JP. Microscale technologies for tissue engineering and biology. Proc Natl Acad Sci USA 2006;103:2480–2487.
5. Hutmacher DW. Scaffolds in tissue engineering bone and cartilage. Biomaterials 2000;21:2529–2543.
6. Mikos AG, Lyman MD, Freed LE, Langer R. Wetting of poly(L-lactic acid) and poly(DL-lactic-*co*-glycolic acid) foams for tissue culture. Biomaterials 1994;15:55–58.
7. Traversa E, Mecheri B, Mandoli C, Soliman S, Rinaldi A, Licoccia S, Forte G, Pagliari F, Pagliari S, Carotenuto F, Minieri M, Nardo P. Tuning hierarchical architecture of 3D polymeric scaffolds for cardiac tissue engineering. J Exp Nanosci 2008;3:97–110.
8. Mooney DJ, Baldwin DF, Suh NP, Vacanti JP, Langer R. Novel approach to fabricate porous sponges of poly(-lactic-*co*-glycolic acid) without the use of organic solvents. Biomaterials 1996;17: 1417–1422.
9. Kim HD, Bae EH, Kwon IC, Pal RR, Nam JD, Lee DS. Effect of PEG-PLLA diblock copolymer on macroporous PLLA scaffolds by thermally induced phase separation. Biomaterials 2004;25: 2319–2329.
10. Chen VJ, Ma PX. The effect of surface area on the degradation rate of nano-fibrous poly(L-lactic acid) foams. Biomaterials 2006; 27:3708–3715.
11. Eichhorn SJ, Sampson WW. Statistical geometry of pores and statistics of porous nanofibrous assemblies. J R Soc Interface 2005;2: 309–318.
12. Thandavamoorthy S, Bhat GS, Tock RW, Parameswaran S, Ramkumar SS. Electrospinning of nanofibers. J Appl Polym Sci 2005;96:557–569.
13. Boland ED, Pawlowski KJ, Barnes CP, Simpson DG, Wnek GE, Bowlin GL. Electrospinning of bioresorbable polymers for tissue engineering scaffolds. In: Reneker DH, Fong H, editors. Polymeric Nanofibers, North Carolina: Oxford University Press; 2006. p188–204.
14. Simpson DG, Bowlin GL. Tissue-engineering scaffolds: Can we re-engineer mother nature? Exp Rev Med Dev 2006;3:9–15.
15. Barnes CP, Sell SA, Boland ED, Simpson DG, Bowlin GL. Nanofiber technology: Designing the next generation of tissue engineering scaffolds. Adv Drug Deliv Rev 2007;59:1413–1433.
16. Huang ZM, Zhang YZ, Kotaki M, Ramakrishna S. A review on polymer nanofibers by electrospinning and their applications in nanocomposites. Compos Sci Technol 2003;63:2223–2253.
17. Pham QP, Sharma U, Mikos AG. Electrospun poly(Îµ-caprolactone) microfiber and multilayer nanofiber/microfiber scaffolds: Characterization of scaffolds and measurement of cellular infiltration. Biomacromolecules 2006;7:2796–2805.
18. Zhu X, Cui W, Li X, Jin Y. Electrospun fibrous mats with high porosity as potential scaffolds for skin tissue engineering. Biomacromolecules 2008;9:1795–1801.
19. Mikos AG, Sarakinos G, Lyman MD, Ingber DE, Vacanti JP, Langer R. Prevascularization of porous biodegradable polymers. Biotechnol Bioeng 1993;42:716–723.
20. Hollister SJ, Maddox RD, Taboas JM. Optimal design and fabrication of scaffolds to mimic tissue properties and satisfy biological constraints. Biomaterials 2002;23:4095–4103.
21. McGlohorn JB, Holder WD Jr, Grimes LW, Thomas CB, Burg KJ. Evaluation of smooth muscle cell response using two types of porous polylactide scaffolds with differing pore topography. Tissue Eng 2004;10:505–514.
22. Uebersax L, Hagenmuller H, Hofmann S, Gruenblatt E, Muller R, Vunjak-Novakovic G, Kaplan DL, Merkle HP, Meinel L. Effect of scaffold design on bone morphology in vitro. Tissue Eng 2006;12: 3417–3429.
23. Balguid A, Mol A, van Marion MH, Bank RA, Bouten CV, Baaijens FP. Tailoring fiber diameter in electrospun poly(varepsilon-caprolactone) scaffolds for optimal cellular infiltration in cardiovascular tissue engineering. Tissue Eng Part A 2009;15: 437–444.
24. Badami AS, Kreke MR, Thompson MS, Riffle JS, Goldstein AS. Effect of fiber diameter on spreading, proliferation, and differentiation of osteoblastic cells on electrospun poly(lactic acid) substrates. Biomaterials 2006;27:596–606.
25. Sell S, Barnes C, Simpson D, Bowlin G. Scaffold permeability as a means to determine fiber diameter and pore size of electrospun fibrinogen. J Biomed Mater Res A 2008;85A:115–126.
26. Kim G, Kim W. Highly porous 3D nanofiber scaffold using an electrospinning technique. J Biomed Mater Res B Appl Biomater 2007;81:104–110.
27. Chen M, Patra PK, Warner SB, Bhowmick S. Role of fiber diameter in adhesion and proliferation of NIH 3T3 fibroblast on electrospun polycaprolactone scaffolds. Tissue Eng 2007;13: 579–587.
28. Woodward SC, Brewer PS, Moatamed F, Schindler A, Pitt CG. The intracellular degradation of poly(ε-caprolactone). J Biomed Mater Res 1985;19:437–444.
29. Li M, Guo Y, Wei Y, MacDiarmid AG, Lelkes PI. Electrospinning polyaniline-contained gelatin nanofibers for tissue engineering applications. Biomaterials 2006;27:2705–2715.
30. Hwang CM, Park Y, Park JY, Lee K, Sun K, Khademhosseini A, Lee SH. Controlled cellular orientation on PLGA microfibers with defined diameters. Biomed Microdev 2009;11:739–746.
31. Tian F, Hosseinkhani H, Hosseinkhani M, Khademhosseini A, Yokoyama Y, Estrada GG, Kobayashi H. Quantitative analysis of cell adhesion on aligned micro- and nanofibers. J Biomed Mater Res A 2008;84:291–299.
32. Moroni L, Licht R, de Boer J, de Wijn JR, van Blitterswijk CA. Fiber diameter and texture of electrospun PEOT/PBT scaffolds influence human mesenchymal stem cell proliferation and morphology, and the release of incorporated compounds. Biomaterials 2006;27:4911–4922.
33. Bashur CA, Dahlgren LA, Goldstein AS. Effect of fiber diameter and orientation on fibroblast morphology and proliferation on electrospun poly(D,L-lactic-*co*-glycolic acid) meshes. Biomaterials 2006;27:5681–5688.